Defective calcium inactivation causes long QT in obese insulin-resistant rat

Yen-Chang Lin, Jianying Huang, Hong Kan, Vincent Castranova, Jefferson C. Frisbee and Han-Gang Yu

Am J Physiol Heart Circ Physiol 302:H1013-H1022, 2012. First published 23 December 2011; doi:10.1152/ajpheart.00837.2011

Am J Physiol Heart Circ Physiol 302: H1013–H1022, 2012.
First published December 23, 2011; doi:10.1152/ajpheart.00837.2011.

Defective calcium inactivation causes long QT in obese insulin-resistant rat

Yen-Chang Lin,[1]* Jianying Huang,[1]* Hong Kan,[2] Vincent Castranova,[2] Jefferson C. Frisbee,[1] and Han-Gang Yu[1]

[1]*Center for Cardiovascular and Respiratory Sciences, Department of Physiology and Pharmacology, Robert C. Byrd Health Sciences Center, West Virginia University, Morgantown; and* [2]*Pathology and Physiology Research Branch, National Institute for Occupational Safety and Health/Centers for Disease Control, Morgantown, West Virginia*

Submitted 24 August 2011; accepted in final form 12 December 2011

Lin Y, Huang J, Kan H, Castranova V, Frisbee JC, Yu H. Defective calcium inactivation causes long QT in obese insulin-resistant rat. *Am J Physiol Heart Circ Physiol* 302: H1013–H1022, 2012. First published December 23, 2011; doi:10.1152/ajpheart.00837.2011.—The majority of diabetic patients who are overweight or obese die of heart disease. We suspect that the obesity-induced insulin resistance may lead to abnormal cardiac electrophysiology. We tested this hypothesis by studying an obese insulin-resistant rat model, the obese Zucker rat (OZR). Compared with the age-matched control, lean Zucker rat (LZR), OZR of 16–17 wk old exhibited an increase in QTc interval, action potential duration, and cell capacitance. Furthermore, the L-type calcium current (I_{CaL}) in OZR exhibited defective inactivation and lost the complete inactivation back to the closed state, leading to increased Ca^{2+} influx. The current density of I_{CaL} was reduced in OZR, whereas the threshold activation and the current-voltage relationship of I_{CaL} were not significantly altered. L-type Ba^{2+} current (I_{BaL}) in OZR also exhibited defective inactivation, and steady-state inactivation was not significantly altered. However, the current-voltage relationship and activation threshold of I_{BaL} in OZR exhibited a depolarized shift compared with LZR. The total and membrane protein expression levels of Cav1.2 [pore-forming subunit of L-type calcium channels (LTCC)], but not the insulin receptors, were decreased in OZR. The insulin receptor was found to be associated with the Cav1.2, which was weakened in OZR. The total protein expression of calmodulin was reduced, but that of Cavβ2 subunit was not altered in OZR. Together, these results suggested that the 16- to 17-wk-old OZR has *1*) developed cardiac hypertrophy, *2*) exhibited altered electrophysiology manifested by the prolonged QTc interval, *3*) increased duration of action potential in isolated ventricular myocytes, *4*) defective inactivation of I_{CaL} and I_{BaL}, 5) weakened the association of LTCC with the insulin receptor, and *6*) decreased protein expression of Cav1.2 and calmodulin. These results also provided mechanistic insights into a remodeled cardiac electrophysiology under the condition of insulin resistance, enhancing our understanding of long QT associated with obese type 2 diabetic patients.

obesity; insulin resistance; long QT; action potential; L-type calcium current; calmodulin

OBESITY IS DIRECTLY LINKED to type 2 diabetes, which has become an increasingly public health problem. In 2004, heart disease was noted on 65–68% of diabetes-related death among people aged 65 years and older (statistics from American Diabetes Association and American Heart Association). Obesity is also a significant contributor to insulin resistance, which is the main feature that occurs early and contributes to the development of diabetes. Cardiac ventricular dysfunction, concomitant with ventricular hypertrophy, is manifested in obese diabetics. Hypertrophied cardiomyocytes are prone to arrhythmias. It may be not coincidental that the major heart diseases associated with diabetic patients are cardiac arrhythmias (26, 39), leading to ventricular dysfunction. Abnormal diastolic left ventricular function in the diabetic heart has been recognized for many years without understanding of the molecular mechanism (22). Recently, evidence for impaired calcium homeostasis in the diabetic heart provides an intriguing mechanism that can directly cause ventricular dysfunction (23).

Ca^{2+} entry is mediated by L-type calcium channels (LTCC) in the ventricular myocytes. In an insulin-deficient mouse model, L-type calcium current (I_{CaL}) has been shown to be reduced in the ventricular myocytes (25). The suppressed phosphatidylinositol 3-kinase (PI3K) signaling was proposed to mediate the reduced cell surface expression of LTCC, providing an explanation for the weakened cardiac contractility in this mouse model (25). Additionally, the expression levels of key calcium-handling proteins have been shown to be either reduced (sodium/calcium exchanger, ryanodine receptor, sarco/endoplasmic reticulum Ca^{2+}-ATPase) or increased (phospholamban) (23). In contrast, there is a paucity of research in cardiac electrophysiology remodeling under insulin-resistant conditions.

Obesity creates a condition for a worsening state, diabetes. One major feature in obesity is the insulin resistance that must result from the defective insulin signaling. Insulin resistance is a multifaceted syndrome that causes not only an impaired glucose regulation but also a number of other diseases at different organs, including dysfunctional cardiac ventricular contraction. Using 16- to 17-wk-old obese Zucker rats (OZR) as an animal model, the purpose of this work was to begin understanding of cardiac arrhythmogenesis directly linked to the sudden cardiac arrest in obese diabetic patients.

MATERIALS AND METHODS

Electrocardiogram recording. Isoflurane (2%) mixed with oxygen at the flow rate of 2 l/min inhaled by OZR and lean Zucker rats (LZR) was used for anesthetization in accordance with Animal Care and Use Committee guidelines for the measurement of electrocardiogram (ECG). ECG was recorded by using a two leads vector. Values for ECG measures are derived by 1-KHz sampling rate. All results are repeated eight times.

Cardiac tissue and myocyte preparation. LZR and OZR at 16–17 wk of age were killed by intraperitoneal injection of pentobarbital in accordance with the Institutional Animal Care and Use Committee protocols. The heart was excised, and ventricles were cut out and prepared for protein chemistry experiments. The ventricular myocytes were prepared using a collagenase dissociation protocol as described previously (19). Briefly, the aorta was cannulated, and the heart was perfused with oxygenated Ca^{2+}-free Tyrode solution at 37°C for 5 min, followed by oxygenated Ca^{2+}-free Tyrode solution containing

* Y.-C. Lin and J. Huang contributed equally to this work.

Address for reprint requests and other correspondence: H.-G. Yu, Center for Cardiovascular and Respiratory Sciences, Dept. of Physiology and Pharmacology, Robert C. Byrd Health Sciences Center, West Virginia Univ., Morgantown, WV 26056 (e-mail: hyu@hsc.wvu.edu).

0.6 mg/ml collagenase II (Worthington) for 20–30 min. The ventricles were minced into small pieces in Krafte-Brühe (KB) solution, dispersed, and filtrated through a 200-μm mesh. The isolated myocytes were stored in KB solution at room temperature for 1 h before patch-clamp experiments. The animal protocols in this study were reviewed and approved by the Institutional Animal Care and Use Committee at West Virginia University and the National Institute for Occupational Safety and Health at Morgantown, WV.

Whole cell patch-clamp studies of action potential and I_{CaL}. Whole cell patch-clamp studies were carried out for action potential and I_{CaL} properties in ventricular myocytes isolated from OZR and LZR at the temperature of 35–37°C. The bath chamber temperature was controlled by a temperature controller (Cell MicroControls). Action potential was recorded at current-clamp mode with normal Tyrode and pipette solutions. The Tyrode solution contains (in mM): 143 NaCl, 5.4 KCl, 1.8 $CaCl_2$, 0.5 $MgCl_2$, 0.25 NaH_2PO_4, and 5 HEPES; pH was adjusted to 7.4 by NaOH. The pipette solution contains (in mM): 120 KCl, 1 $CaCl_2$, 5 $MgCl_2$, 5 Na_2ATP, 11 EGTA, 10 HEPES, and 11 glucose; pH was adjusted to 7.3 by KOH. The current stimulus was 1 nA for 2–5 ms.

I_{CaL} currents (Ca^{2+} were used as the charge carrier) and I_{BaL} currents (Ba^{2+} were used as the charge carrier) were recorded in the solutions similar to that of a previous report with no Na^+ and K^+ in both pipette and bath solutions (24). For I_{CaL} recordings, the pipettes had a resistance of 2–5 MΩ when filled (in mM): 108 CsCl, 4 $MgCl_2$, 9 EGTA, and 9 HEPES. The bath solution contained (in mM): 2 $CaCl_2$, 1 $MgCl_2$, 10 HEPES, 40 TEA, 10 glucose, and 65 CsCl. For I_{BaL} recordings, 2 mM $BaCl_2$ was used to replace $CaCl_2$. Both pipette and bath solutions were adjusted by CsOH to pH 7.2. P/4 protocols were used to remove the leak currents. The I_{CaL} and I_{BaL} were conducted in different myocytes. For I_{CaL} recording, eight myocytes were repeated for each group, whereas at least five myocytes were repeated in I_{BaL} recordings. The capacitive currents were minimized with 75–85% series resistance compensation.

Data were collected by Clampex (8.0) using an Axon 200B amplifier. Data analysis was performed using Clampfit (8.0). The statistical analysis was performed by Student's *t*-test. The averaged data were presented as means ± SE.

Total and membrane protein preparation, Western blots, and coimmunoprecipitation. The ventricular tissue removed from OZR and LZR hearts was pulverized under liquid nitrogen and homogenized in buffer containing 20 mM Tris, 150 mM NaCl, 10 mM EGTA, and 10 mM EDTA (pH 7.4), supplemented with protease inhibitors. After centrifuge at 10,000 *g* at 4°C to remove debris, the supernatant was subjected to ultracentrifugation at 100,000 *g* (4°C) for 1 h. Membrane proteins were collected as pellets after ultracentrifugation and solubilized in homogenization buffer plus 1% digitonin for 30 min at 4°C. Protein concentration was determined using BCA or Bradford assay. For immunoprecipitation experiments, equal amounts of total protein (0.5–1 mg) were incubated with a specific antibody (2–4 μg) for 1 h at 4°C, and 30–50 μl protein A/G PLUS-agarose (Santa Cruz) was then added and incubated overnight with gentle rocking. The beads were washed extensively with cold PBS buffer and resuspended in 2× sample buffer. The immune complexes were separated by SDS-PAGE and analyzed by Western blot using the specific antibody of interest. Total protein of 5–20 μg/sample was subjected to SDS-PAGE using 4–12% gradient gels (Invitrogen) and then transferred to nitrocellulose membranes (Amersham) and incubated with proper antibodies [anti-α_{1C} (Millipore/Alomone); anti-$Cav\beta_2$ (University of California Davis); anti-calmodulin (Cell Signaling), and anti-IR-β generously provided by Dr. Martin Myers]. It is noticed that the specificity and quality of α_{1C} antibodies are not perfect, which are also noticed by the vendors (Millipore and Alomone). Both low- and high-molecular weight forms of α_{1C} are detected (e.g., see Fig. 7*C*). After being washed and incubated with horseradish peroxidase-conjugated secondary antibody, immunoreactive proteins were visualized with the SuperSignal West Pico kit (Pierce). All protein experiments were repeated at least three times, if not mentioned in the text.

RESULTS

ECG and increased size of ventricular myocytes in OZR. Figure 1*A* shows the representative lead II ECG recordings from a 16-wk-old OZR and an age-matched LZR. The enlarged ECGs depicting the ECG characteristics are shown in Fig. 1*A*, *right*. Compared with LZR, the averaged corrected QT interval (QTc) is prolonged by 22% (LZR: 123 ± 3 ms, $n = 8$; OZR: 153 ± 9 ms, $n = 8$), shown in Fig. 1*B*. Additionally, the T wave of OZR is enhanced, and the descending limb of the T wave is increased. We used the QTc-Fridericia approach for QTc measurement, which has been widely used at fast heart rates and produces more consistent results (16).

To assess the potential hypertrophied heart that associates with the altered ECG, we studied cell capacitance (Cm) of isolated single ventricular myocytes. Cell capacitance directly reflects the cell volume. Figure 1*C* shows that the isolated ventricular myocytes were 37.9% larger in OZR than in LZR (Cm_LZR: 94.5 ± 4.3 pF, Cm_OZR: 130.7 ± 5.7 pF, $P < 0.0001$).

Action potentials of LZR and OZR ventricular myocytes. Figure 2 shows the representative recordings of action potentials in ventricular myocytes isolated from 16-wk-old LZR (Fig. 2*A*) and OZR (Fig. 2*B*) as well as Sprague Dawley (SD) rat (Fig. 2*C*) hearts. LZR action potential is close to that of SD rat (43). OZR action potential, however, exhibited a remarkable plateau phase similar to those in canine (42) and human (18, 35) ventricles. On average of 10 myocytes for LZR and OZR, respectively, the duration of APD_{90} (measured at the 90% of action potential amplitude from the peak potential) is increased by over twofold in OZR compared with LZR (LZR: 91.5 ± 4.6 ms, $n = 10$; OZR: 199.8 ± 11.2 ms, $n = 10$) (Fig. 2*D*).

I_{CaL} in isolated ventricular myocytes. Prolonged QT interval results from either an increased inward ionic flow, a decreased outward current, or a combination of both. We focused on the LTCCs because of its primary role in Ca^{2+} influx. Figure 3*A* shows the representative currents of I_{CaL} recorded at +10 mV in ventricular myocytes isolated from a 16-wk-old OZR compared with an age-matched LZR heart. I_{CaL} inactivation was apparently disrupted in OZR compared with LZR. The I_{CaL} currents from both LZR and OZR myocytes were confirmed by blockade of 10 μM verapamil.

Because of the disrupted inactivation of I_{CaL}, the Ca^{2+} influx at 0 mV, calculated from the area enclosed by activation and inactivation of I_{CaL} as well as the zero current line, was increased by 43 ± 12% in OZR compared with LZR ($P = 0.002$, $n = 8$) (Fig. 3*B*).

Figure 4 shows the representative currents illustrating the disrupted I_{CaL} inactivation in OZR compared with LZR. At the potentials of −40 and −30 mV, I_{CaL} has little inactivation in OZR (Fig. 4*B*). At −20 mV, the OZR I_{CaL} does inactivate, but not as complete as LZR I_{CaL} (Fig. 4*A*). The fraction of residual currents remaining at the end of 400 ms to the step (R_{400}) was plotted against the test potentials and shown in Fig. 4*C*. Ca^{2+} dependence of I_{CaL} inactivation is dramatically attenuated in OZR compared with LZR. The voltage-dependent inactivation kinetics were shown in Fig. 4*D*. The inactivation was best fit by a two-component exponential function (Fig. 4*D*). The kinetics

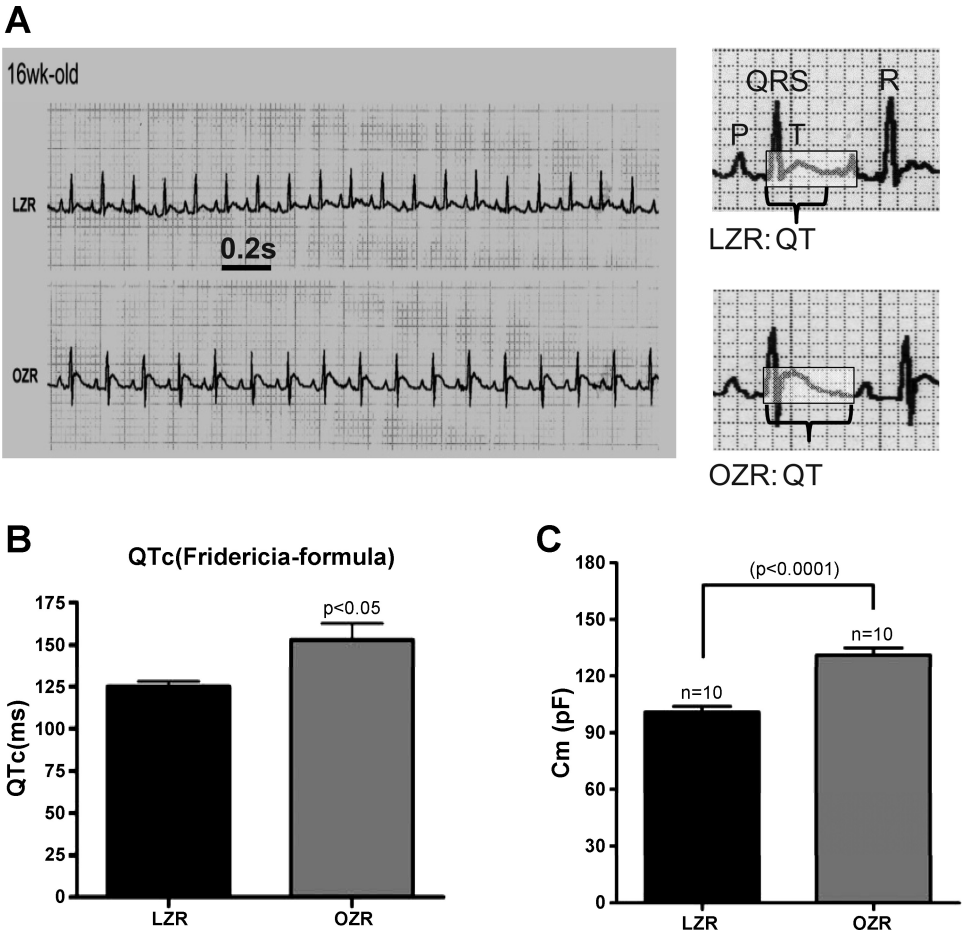

Fig. 1. Electrocardiography (ECG) and cell size in obese Zucker rats (OZR) compared with lean Zucker rats (LZR). *A*: ECG recorded at lead II for 16-wk-old LZR (*top*) and OZR (*bottom*). *Right*, enlarged ECGs depicting the main peaks and QT intervals for LZR and OZR. *B*: corrected QT (QTc) interval was prolonged from 16-wk-old OZR compared with LZR; $n = 8$ for OZR and LZR. *C*: averaged results for capacitance measurement (Cm) in LZR and OZR myocytes ($n = 10$).

of the fast component of inactivation in OZR are not significantly different from LZR at negative voltages but significantly slower at positive voltages near the plateau of action potential compared with LZR. The kinetics of the slow component of inactivation, however, are much slower in OZR than in LZR.

Figure 5 shows that the current-voltage relationship of I_{CaL} activation is unaltered in OZR (Fig. 5*A*). However, the I_{CaL} current density was decreased in OZR myocytes compared with LZR (at +10 mV, LZR: 10.2 ± 0.4 pA/pF; OZR: 8.4 ± 0.5 pA/pF; $P < 0.05$, $n = 8$ for each group). Figure 5*B* shows the voltage-dependent activation curves derived from the current-voltage relationships of Fig. 5*A*. Boltzmann fit revealed the midpoint voltage of activation of −25.8 ± 1.2 mV ($n = 8$) for LZR and −31.9 ± 7.4 mV ($n = 8$) for OZR. The difference is statistically insignificant ($P > 0.05$). Figure 5*C* shows that, using a two-pulse protocol (41), the I_{CaL} steady-state inactivation curve was not significantly shifted in OZR (gray line) compared with LZR (dark line) ($V_{1/2}$_LZR: −27.5 ± 3 mV, $V_{1/2}$_OZR: −31.1 ± 2 mV, $n = 6$, $P > 0.05$).

When Ba^{2+} was used as a charge carrier, disrupted inactivation of I_{Ba} is still present (Fig. 6*A*) in OZR. The current density was reduced, especially near the peak, which is shifted to depolarized potential for OZR (+20 mV compared with +10 mV for LZR) (Fig. 6*B*). The voltage-dependent activation curve of I_{Ba} is also shifted to more positive potential for OZR compared with LZR (Fig. 6*C*) ($V_{1/2}$_LZR: −11.7 ± 4 mV, $V_{1/2}$_OZR: 3.4 ± 4 mV, $n = 5$, $P < 0.05$). The steady-state inactivation is not significantly altered ($V_{1/2}$_LZR: −19.6 ± 3 mV, $V_{1/2}$_OZR: −17.1 ± 5 mV, $n = 5$, $P > 0.05$).

Association of insulin receptor and LTCC protein (Cav1.2). If the altered I_{CaL} results from the impaired insulin regulation, the LTCC and the insulin signaling molecules should be close beneath the plasma membrane. Figure 7 shows that the insulin receptor and the pore-forming subunit of LTCC (Cav1.2) are indeed associated with each other in the rat ventricle. Using an antibody against the β-subunit of insulin receptor (IR-β antibody, generously provided by Dr. Martin Myers from the University of Michigan), we first verified the presence of the insulin receptor expression in SD rat ventricles (Fig. 7*A*). We then precipitated the sample using a Cav1.2 antibody and detected insulin receptor signals using the IR-β antibody (Fig. 7*B*). If we precipitated the sample using the IR-β antibody, the Cav1.2 signals were also detected using the Cav1.2 antibody (Fig. 7*C*). The double bands of α_{1C} are presumably due to the glycosylation of the channel proteins in the heart, and observed by others using the same α_{1C} antibody (13). Absence of IR immunoblots after immunoprecipitation with a hyperpolarization-activated cation channel (HCN) 3 antibody was used as negative controls, since HCN3 is absent in the heart (32). We have previously used the same α_{1C} antibody to identify the association of α_{1C} with HCN2, a cardiac pacemaker channel (24) that served as a positive control.

We extended the coimmunoprecipitation experiments to OZR to study whether the associated IR and Cav1.2 might be

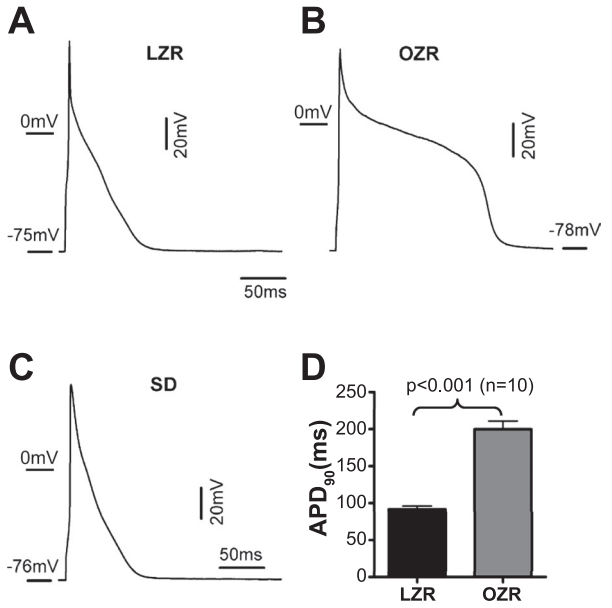

Fig. 2. Action potential durations in OZR, LZR, and Sprague Dawley (SD) rat. Action potentials recorded in isolated ventricular myocytes from LZR (*A*), OZR (*B*), and SD (*C*). Averaged action potential duration measured at 90% (APD_{90}) of action potential amplitude from the peak potential is shown in *D*.

changed. Figure 8 shows that the association is weakened in OZR compared with LZR (Fig. 8*B*), although the expression levels of insulin receptors are unaltered in OZR (Fig. 8*A*). The similar results were repeated in an additional four pairs of rat hearts. The quantitative analysis revealed a 43% weaker IRβ signal in OZR compared with LZR (Fig. 8*C*). These results highly suggested an altered protein expression in the Cav1.2 complex in OZR ventricles. Multiple bands of the β-subunit of insulin receptor have also been observed by others (26).

Reduced expression of Cav1.2 and calmodulin in OZR. Figure 9 shows that indeed the total Cav1.2 protein expression was reduced in OZR ventricles (Fig. 9*A*). On average, the total Cav1.2 protein levels (260 + 95 kDa) were decreased by 47 ± 14% compared with LZR (Fig. 9*C*). Negative and positive controls are shown in Fig. 9, *B* and *D*, respectively. The total membrane protein expression levels of Cav1.2 were also decreased in OZR compared with LZR, shown in Fig. 10*A*. Averaging over six repeated experiments, the OZR total membrane protein levels of Cav1.2 (260 + 95 kDa) were reduced by 55 ± 7% compared with LZR (Fig. 10*B*). Furthermore, the ratio of signals at 260 kDa over that at 95 kDa was significantly increased in OZR (r_LZR: 0.45 ± 0.07, r_OZR: 0.82 ± 0.04, $n = 6$, $P < 0.05$) (Fig. 10*C*).

Calmodulin and the regulatory Cavβ2 subunit have been demonstrated to be key molecules that determine *1*) inactivation (10), *2*) cell surface expression (10), and *3*) protein stability of Cav1.2 (4). Thus, we also examined the protein expression of these two molecules in OZR. Figure 11*A* shows the protein expression levels of Cavβ2 and calmodulin in OZR and LZR. On average of five hearts for each group, Cavβ2 protein expression levels were barely changed in OZR, but the calmodulin protein levels were significantly decreased in OZR (27 ± 8%, $n = 5$, $P < 0.05$) compared with LZR ventricles (Fig. 11*B*). Consistently, application of a specific calmodulin blocker, W-7 (15 μM), for 15–30 min significantly slowed inactivation and inhibited the current amplitude of LZR I_{CaL} (Fig. 11*C*), which mimicked the abnormal I_{CaL} in OZR (Fig. 3*A*).

DISCUSSION

In this study, we focused on the impaired gating properties of I_{CaL} by the pathological state, collectively called metabolic syndrome, that is induced by obesity, in the 16- to 17-wk-old OZR (17). Enlarged myocytes (Fig. 1*C*) indicated a hypertrophied heart at this age, in response to increased arterial pressure and total peripheral resistance (29).

We detected a prolonged QTc interval in OZR compared with the age-matched LZR (Fig. 1). Not surprisingly, we found a significantly increased duration of action potential in OZR myocytes compared with LZR myocytes (Fig. 2). What is surprising is the apparent plateau phase that has never been observed in rat ventricles. The underlying ionic mechanisms of the plateau phase are complex and well understood (30). It is unlikely that the dramatic change in OZR action potential compared with LZR is caused by alteration of one channel or exchanger protein. Increased I_{CaL} is one of the underlying ionic

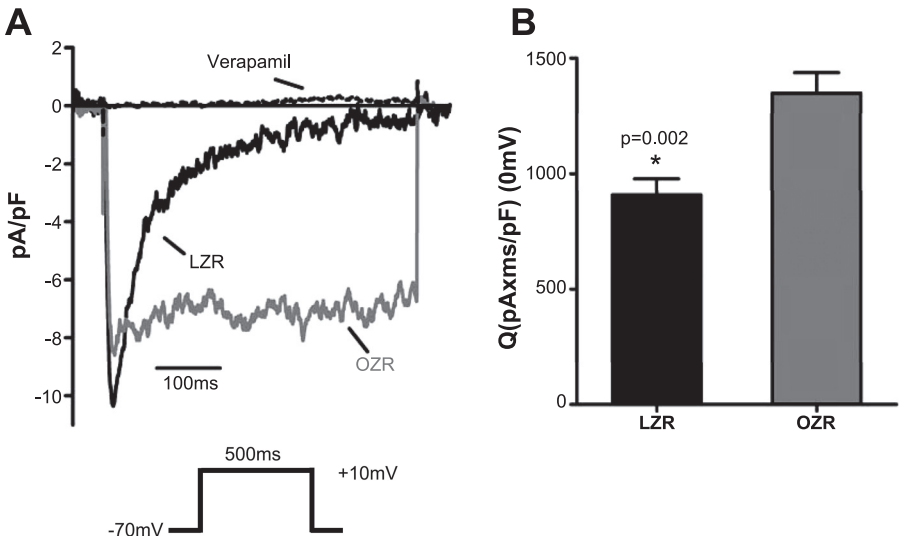

Fig. 3. L-type calcium current (I_{CaL}) inactivation and Ca^{2+} influx in ventricular myocytes from OZR and LZR. *A*: I_{CaL} elicited by 500-ms depolarizing pulse to +10 mV in OZR (gray line) and LZR (dark line) myocytes. Holding potential was −70 mV. The pulse protocol is shown below. Both OZR and LZR I_{CaL} were verified by application of 10 μM verapamil (broken line). *B*: Ca^{2+} influx calculated from the area enclosed by I_{CaL} and zero current line recorded at 0 mV. The influx was normalized by the cell size. The data were averaged from 8 myocytes for each group. *Difference between LZR and OZR Ca^{2+} influx was statistically significant ($P = 0.002$).

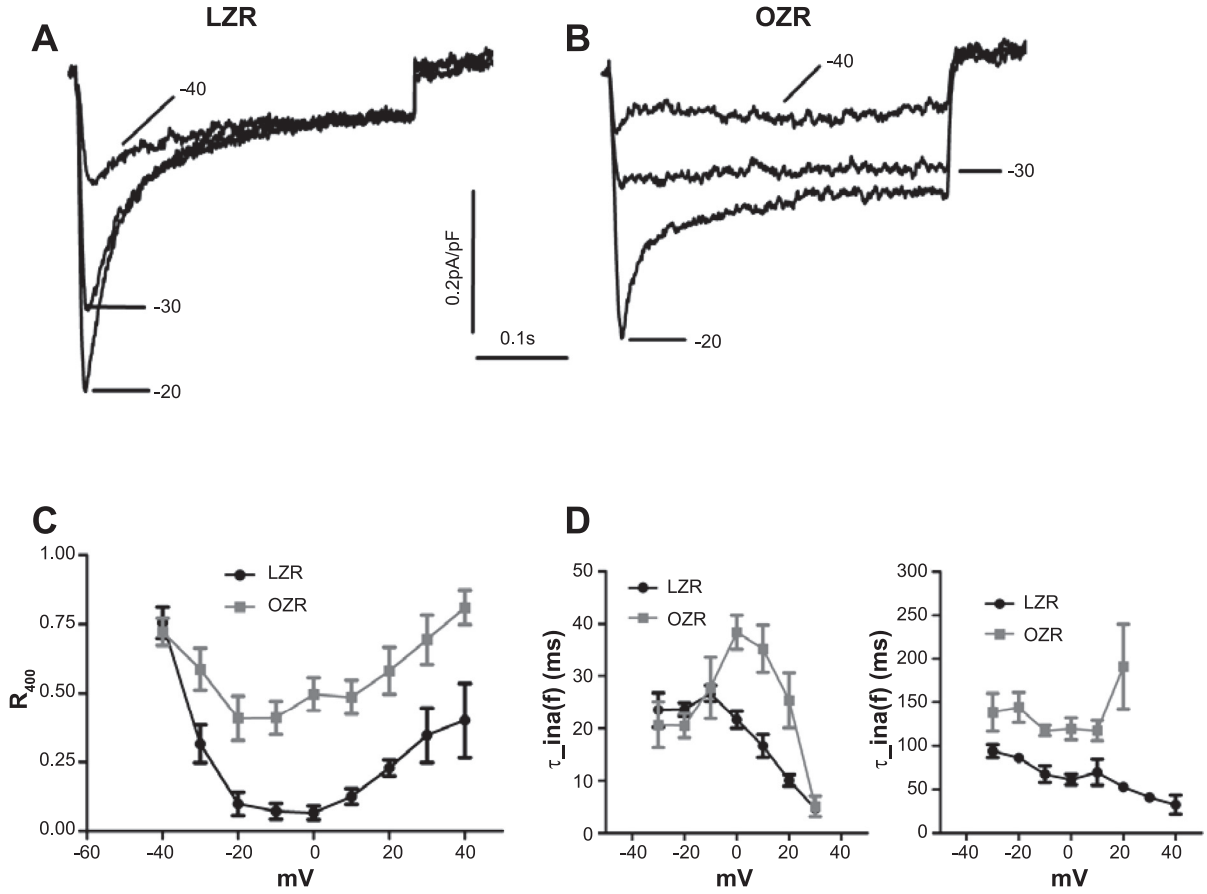

Fig. 4. Disrupted I_{CaL} inactivation in OZR compared with LZR. Representative current traces recorded at indicated voltages in myocytes isolated from LZR (*A*) and OZR (*B*) ventricles. The depolarizing pulse duration was 400 ms. *C*: voltage dependence of the fraction of remaining current at the end of 400 ms into the step (R_{400}) for LZR and OZR. *D*: voltage-dependent inactivation kinetics for LZR and OZR, including the fast component (*left*) and the slow component (*right*).

mechanisms for long QT (15); we thus focused on the potential alteration of I_{CaL} and its underlying mechanisms.

I_{CaL} in OZR ventricular myocyte. We found that I_{CaL} current density is reduced in OZR compared with LZR (Fig. 5*A*). On the other hand, the voltage dependence of I_{CaL} is not altered (Fig. 5, *A* and *B*). More intriguingly, we found a disrupted I_{CaL} inactivation in OZR ventricular myocytes (Fig. 3*A*). I_{CaL} in OZR barely inactivates at negative potentials such as −30 mV (Fig. 4*B*). The slow-component inactivation is much slower, probably reflecting a disrupted calcium-dependent inactivation

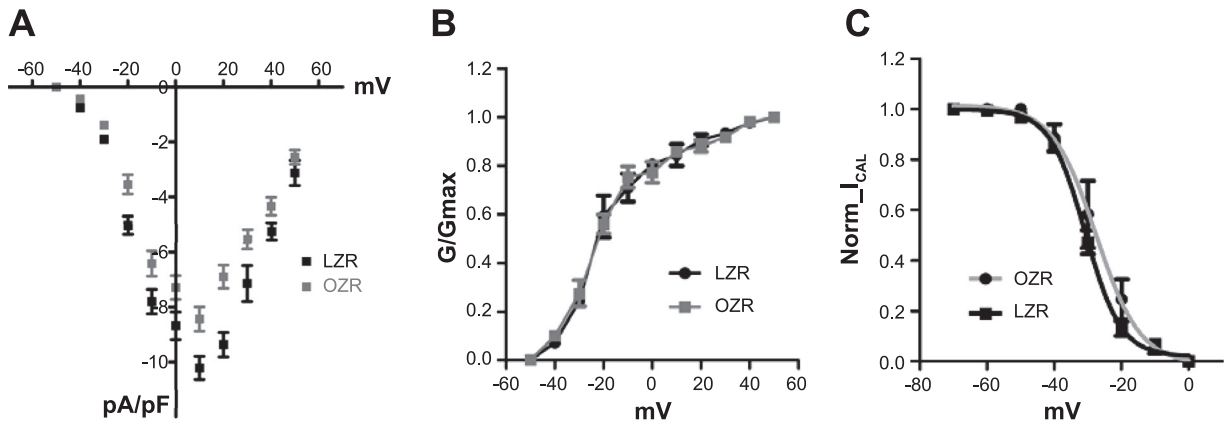

Fig. 5. I_{CaL} gating properties. *A*: current-voltage (*I-V*) relationship of I_{CaL} in OZR and LZR myocytes. *B*: voltage-dependent activation curves (G/G_{max}), derived from *I-V* relationship curves (*A*). Conductance (G) was calculated from the equation, $G = I/(V_m - V_{rev})$, where I is the peak current of I_{CaL}, V_m is the test voltage, and V_{rev} is the reversal potential. The values of V_{rev} were obtained by extrapolating the *I-V* curves. V_{rev} was −69 ± 6 mV for LZR (n = 8) and −74 ± 5 mV for OZR (n = 8), respectively. G_{max} is the maximal conductance. *C*: steady-state inactivation curves of I_{CaL} were obtained using a two-pulse protocol. The conditioning pulses of 500 ms were from −70 to +20 mV in 10-mV increments. After a brief pulse of 5 ms, the test pulse was applied to 10 mV for 300 ms. The holding potential was −70 mV. The data were best fit by a Boltzmann equation to obtain $V_{1/2}$ for the steady-state inactivation curve.

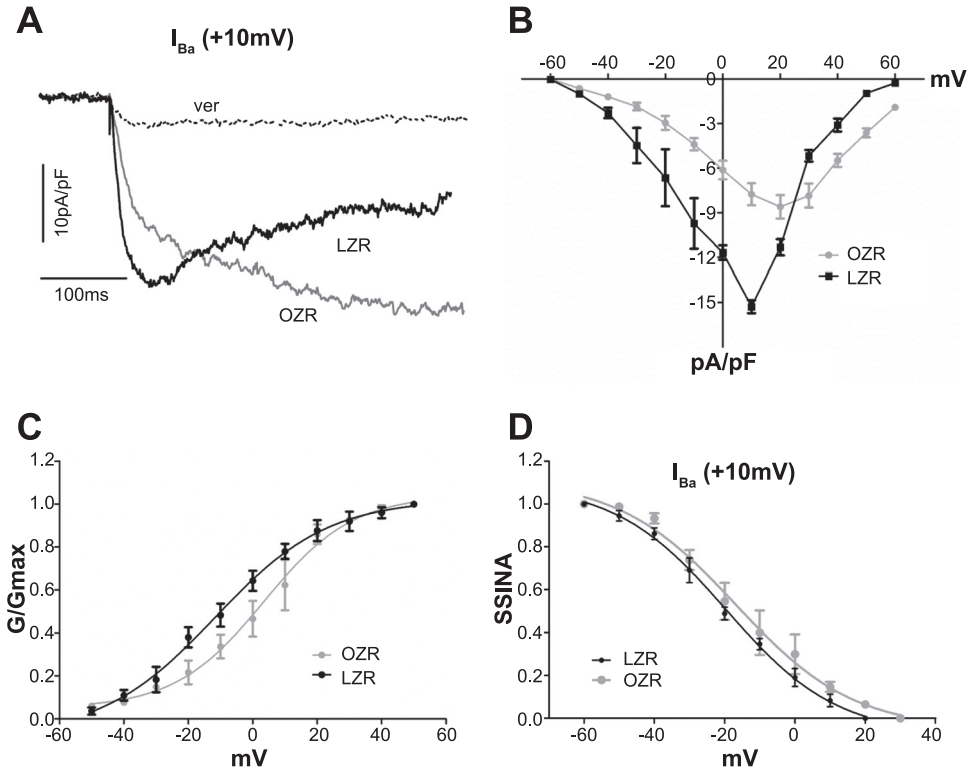

Fig. 6. L-type Ba^{2+} current (I_{BaL}) gating properties. *A*: I_{BaL} traces in response to a depolarizing pulse of 450 ms to +10 mV from the holding potential of −70 mV in a LZR (black) and in an OZR (gray) myocyte, respectively. Both currents were blocked by 10 μM verapamil (broken line). *B*: *I-V* relationship curves of I_{BaL} for LZR (black) and OZR (gray). *C*: activation curves of I_{BaL} for LZR (black) and OZR (gray). *D*: steady-state inactivation (SSINA) curves of I_{BaL} for LZR (black) and OZR (gray). The results were averaged from 5 myocytes for each group.

in OZR (Fig. 4*D*), whereas the fast-component inactivation was slower in OZR at the potentials near the action potential plateau phase, probably indicating the decreased voltage-dependent inactivation in OZR (Fig. 4*D*) (11). Lack of efficient inactivation caused a larger Ca^{2+} influx (Fig. 3*B*), consistent with a much less voltage-dependent change in R_{400} (Fig. 4*C*). A larger Ca^{2+} influx, especially at potentials near 0 mV, can contribute directly to prolonged duration of action potential (Fig. 2*D*) and the QTc interval in OZR (Fig. 1*B*).

The voltage-dependent inactivation of LTCC was also changed (Fig. 6). In addition to the shifted current-voltage relationship for OZR, I_{BaL} also exhibited a depolarized shift of activation, consistent with the shift in the current-voltage relationship. These altered properties were not observed for I_{CaL} in OZR. However, like I_{CaL}, the steady-state inactivation of I_{BaL} was not altered in OZR compared with LZR, indicating the differential voltage- and calcium-dependent regulation in LTCC. The altered LTCC voltage- and calcium-dependent properties can result from a disruptive modulation of the channel expressed at the plasma membrane, an altered protein expression of the channel complex, or both.

Protein expression of Cav1.2, Cavβ2, and calmodulin. Cardiac LTCC is constituted of the pore-forming subunit, Cav1.2 (α_{1C}), β subunit (mainly β_2), and $\alpha_2\delta$ (5, 36). Cav1.2 has four repeats of the six-transmembrane domains with its NH_2- and COOH-termini located inside the cell. The α-interaction domain in the I-II linker is associated with the β-subunit. A disulfide bond links two extracellular α-subunits and the δ-subunit that has one transmembrane domain. Both β- and $\alpha_2\delta$-subunits enhance the membrane trafficking of Cav1.2 and I_{CaL} current density and modulate I_{CaL} inactivation (1, 8, 10). In the COOH-terminal region, critical amino acid residues have been identified for association with calmodulin to form the molec-

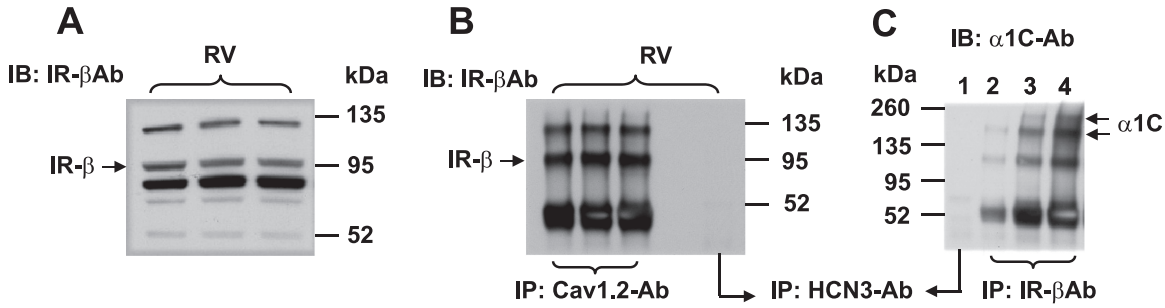

Fig. 7. Association of insulin receptor (IR) with α_{1C} in SD rat ventricles (RV). *A*: IR expression in SD heart. IB, immunoblot. *B*: IR β-subunit signals were readily detected in three separate samples with the IR β-subunit antibody (Ab) after the samples were first immunoprecipitated using an antibody against α_{1C}. HCN, hyperpolarization-activated cation channel. *C*: α_{1C} signals were detected in RV samples with the α_{1C} antibody after the samples were first immunoprecipitated using the IR β-subunit antibody. The amount of IR β-subunit was increased 5-fold (*lane 3*) and 10-fold (*lane 4*) compared with that in *lane 2* to confirm the appearance of α_{1C} signals.

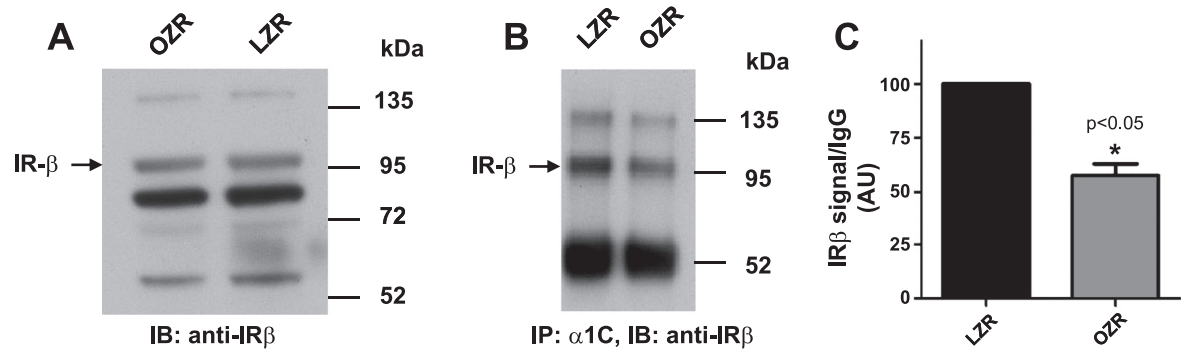

Fig. 8. Association of IR with α_{1C} in OZR and LZR ventricles. *A*: IR protein expression. *B*: IR association with α_{1C} in OZR compared with LZR. The IR β-subunit appeared in calculated molecular weight near 95 kDa. *C*: the intensities of IR β-subunit signals (measured in pixels) near 95 kDa were normalized to IgG for both LZR and OZR and expressed as arbitrary units (AU) ($n = 4$).

ular inactivation machinery, including at least the EF hand, peptide A, C, and the IQ motif (3, 6, 27).

A significant decrease in Cav1.2 protein expression in OZR compared with LZR (Figs. 9*A* and 10*A*) is consistent with the reduced I_{CaL} current density (Fig. 5*A*). The antibody we used can detect two bands of intact Cav1.2 protein near its calculated molecular weight of 260 kDa (Figs. 9*A* and 10*A*). They represent possibly the mature form (posttranslational modification) and immature form (no posttranslational modification) (Alomone). Because of the high proteolytic activity in cardiac (and skeletal) muscle, strong bands at low molecular weight near 95 kDa were detected (Figs. 9*A* and 10*A*). It is noticed that Cav1.2 in both total protein and membrane protein levels was significantly decreased in OZR compared with LZR. It is also found that Cav1.2 has less degradation in OZR than in LZR ventricles as indicated by weaker bands at 95 kDa (Figs. 9*A* and 10*A*). It is worth emphasizing that not all channels expressed at the plasma membrane function at the same time. While the functional channels are better characterized by patch-clamp studies, membrane protein expression provides an overall structural basis for the altered function of LTCC induced by disease.

We have found no changes in protein expression levels of Cavβ2 in OZR compared with LZR. Currently, it is unknown whether the phosphorylation state of Cavβ2 is altered in OZR compared with LZR, since the protein kinase B (Akt)-depen-

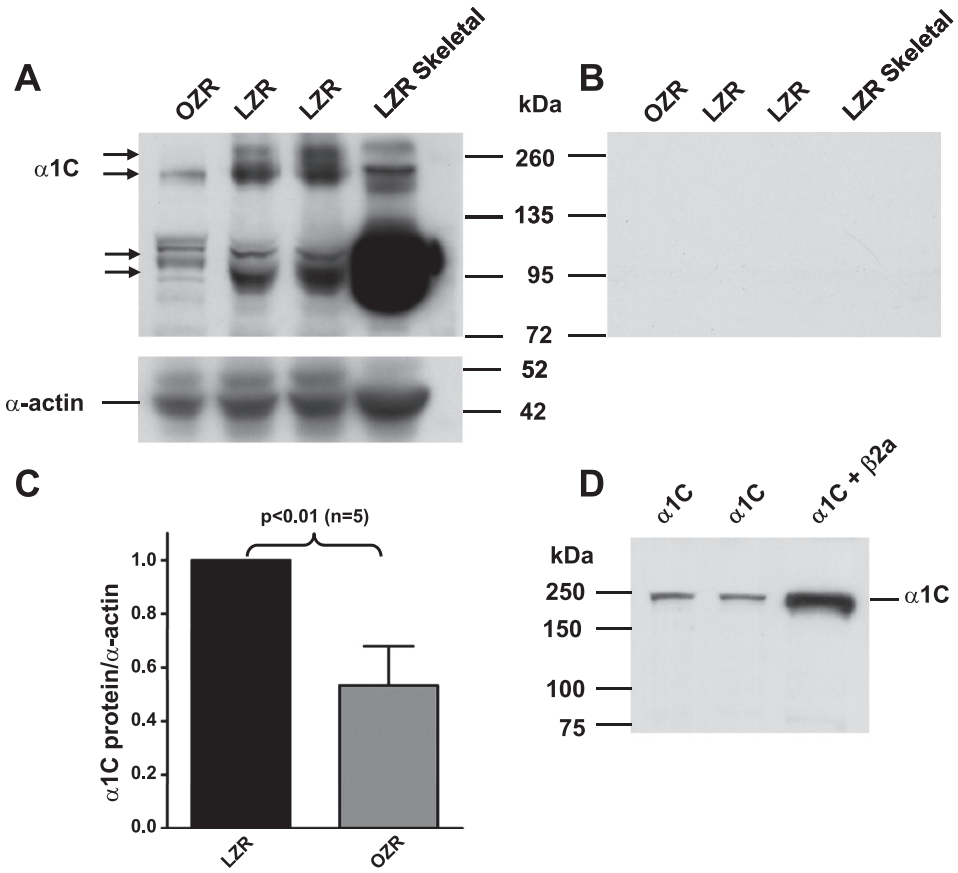

Fig. 9. Cav1.2 (α_{1C}) protein expression in LZR and OZR ventricles. *A*: Cav1.2 (α_{1C}) protein expression in LZR skeletal muscle (serving as a positive control), LZR ventricles (duplicate), and OZR ventricles with a Cav1.2 antibody. *B*: negative control: samples were preincubated with Cav1.2 antigen-peptide 848–865. *C*: %decrease in Cav1.2 protein levels in OZR heart compared with LZR heart. Quantitative measurement of Cav1.2 protein levels was normalized to cardiac-specific α-actin. *D*: Western blotting of full-length Cav1.2 plasmid expressed in the HEK 293 cells served as a positive control showing the lack of proteolysis of Cav1.2 in the HEK 293 cells. It also shows an enhanced protein expression of Cav1.2 by Cavβ2. Equal amount of protein was loaded (30 μg).

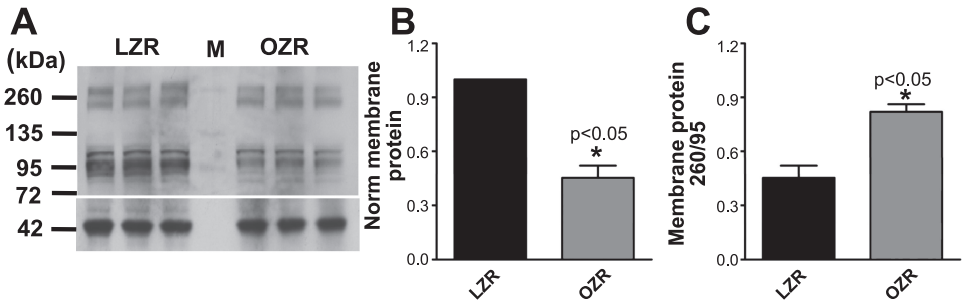

Fig. 10. Cav1.2 membrane protein expression. *A*: membrane protein expression of Cav1.2 in OZR and LZR ventricles. Three repeated data are shown. The α-actin bands (*bottom*) were used as loading controls. M, marker. *B*: average changes in total membrane protein levels of Cav1.2 in OZR (gray) compared with LZR (dark), $n = 6$. The expression levels were normalized to LZR protein level. *C*: average changes in ratio of Cav1.2 signals at 260 kDa (intact) over that at 95 kDa (proteolyzed) in OZR (gray bar) and LZR (dark bar). *Statistical significance ($P < 0.05$) compared with LZR.

dent phosphorylation of Cavβ2 increases the protein stability of Cav1.2 (4). The double band of Cavβ2 (Fig. 11*A*) may be explained by five isoforms in the Cavβ2 family resulting from alternative splicing (12). The difference of these isoforms is located in the NH_2-terminus. The predicted molecular weights of these isoforms vary from each other slightly. Therefore, the double band is likely the result of detecting more than one isoform of Cavβ2 (7).

Intriguingly, the levels of calmodulin protein expression are significantly decreased in OZR (Fig. 11*A*). A decreased calmodulin protein expression explains the impaired voltage- and calcium-dependent I_{CaL} inactivation, which is confirmed by patch-clamp data showing a disrupted inactivation of LZR I_{CaL} in the presence of W-7 (Fig. 11*C*).

Association of insulin receptor and Cav1.2. The common underlying mechanism in type 1 and type 2 diabetes is the impaired insulin signaling, caused by either insufficient release of insulin (type 1) or reduced insulin sensitivity to insulin receptor signaling (type 2). Although OZR is frequently used as an animal model of metabolic syndrome, it is also a good model for studying cardiac insulin resistance (28, 44). As an early event, insulin resistance occurs as early as 7 wk in OZR (9). Even in the late state of metabolic syndrome, insulin resistance remains as a main feature.

Binding of insulin to its receptor activates the receptor's tyrosine kinase activity, leading to the activation of insulin receptor substrate, which, in turn, activates the PI3K/Akt pathway (2). Our coimmunoprecipitation experiments have shown that the insulin receptor is associated with Cav1.2 in the ventricle, and this association is weakened in the OZR compared with LZR (Fig. 8*B*). Because the levels of insulin receptor are unaltered (Fig. 8*A*), the weakened association is likely due to a decreased level of total and membrane protein expression of Cav1.2 (Figs. 9*A* and 10).

Massive effort has been invested in the pathophysiology of diabetes caused by obesity. In the meantime, there is a paucity of research for the altered cardiac electrophysiology that occurs as an early marker associated with insulin resistance. Given the recent realization for a significantly higher risk of sudden cardiac arrest in diabetes, it is essential to understand the underlying mechanisms that predispose the heart to cardiac arrhythmias in obese patients. One of the early and most consistent observations in the heart of diabetics is the prolongation of QTc interval (23). Disrupted I_{CaL} inactivation may cause a long QTc interval, a precursor for sudden cardiac arrest that occurred in patients with type 1 and type 2 diabetes (14, 21), under obese conditions. Prolongation of QTc interval has also been demonstrated as an independent risk factor in type 1 and type 2 diabetes (34, 37, 38), as well as a significant predictor of cardiac death (31, 34). Our work has provided one ionic mechanism: defective I_{CaL} inactivation contributed to the prolonged QTc interval in the OZR heart.

Defective inactivation of I_{CaL} was also found to cause prolonged QT (LQT8) in Timothy Syndrome (33). A mutation was identified at residue 406 with glycine replaced by arginine, creating a missense mutant, G406R, located in the intracellular loop linking domain I and domain II of Cav1.2. G406R exhibited a significant decrease in both calcium- and voltage-dependent inactivations when expressed in Chinese hamster ovary cells and in *Xenopus* oocytes, respectively. The Ca^{2+}

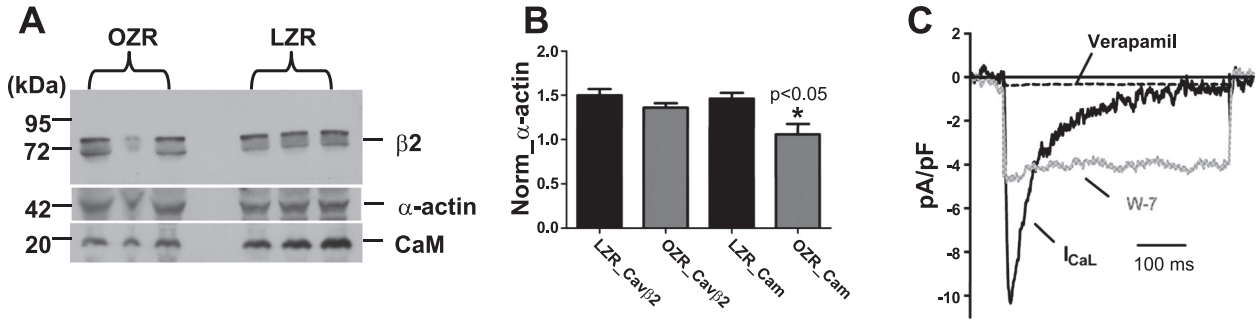

Fig. 11. Protein expression of Cavβ2 and calmodulin (CaM) in OZR and LZR ventricles. Three repeated data are shown in *A*. The middle lane in OZR was ignored due to the distorted signal. The α-actin bands were used as loading controls. *B*: average total protein levels of Cavβ2 and CaM in LZR (dark bar) and OZR (gray bar). Signals were normalized to α-actin. *Statistical significance ($P < 0.05$) compared with LZR. *C*: I_{CaL} at +10 mV in a LZR myocyte (dark line) and the effects of W-7 (gray line). LZR I_{CaL} was verified by 10 μM verapamil (broken line). The holding potential = −50 mV.

current-voltage relationship and the voltage-dependent activation are not significantly altered. Computer simulation predicted a 17% prolongation of ventricular action potential duration, which causes the prolonged QT leading the lethal arrhythmia, the ultimate trigger of death in this disorder (33). Compared with the wild-type I_{CaL}, the alterations induced by G406R are similar to our results, but there are apparent differences. The defective inactivation of Ca^{2+} currents, unchanged current-voltage relationship, and voltage-dependent activation are similar to ours (Figs. 3–5). However, we found that the action potential duration is nearly doubled in OZR myocytes than that in LZR myocytes (Fig. 2), suggesting altered ionic mechanisms in addition to I_{CaL}. Furthermore, the underlying mechanisms for the defective inactivation of I_{CaL} may be different. It is unknown whether mutation in Cav1.2 may occur in OZR. It is known, however, that OZR at 16 wk old is obese and fully developed insulin resistance (17). Our findings of the weakened association of insulin receptor with Cav1.2 and the reduced protein expression of calmodulin provided novel mechanisms for defective inactivation of I_{CaL}. Mechanistic understanding of altered cardiac electrophysiology associated with insulin resistance is also important for potential therapeutic treatment of heart disease in diabetes patients that are overweight. For instance, a cyclin-dependent kinase inhibitor, roscovitine, has recently been found to enhance the voltage-dependent inactivation of Cav1.2 (40), which may be useful to correct the disrupted I_{CaL} inactivation.

While the present work provided mechanistic rationale for some calcium channel blocker to limit the excessive Ca^{2+} influx in the prevention of cardiac remodeling in type 2 diabetes (20), our results also raised many intriguing questions. First, does insulin modulate I_{CaL} gating directly through association of insulin receptor and Cav1.2? Second, are reduced calmodulin protein levels (which can explain the disrupted I_{CaL} inactivation) caused by insulin resistance? Third, will Cavβ2 phosphorylation be affected by impaired insulin signaling? Fourth, is the protein expression of δ-subunit (another integrated regulatory subunit of Cav1.2) altered in OZR? Fifth, is the downstream signaling pathway such as PI3K/Akt involved in the disruptive regulation of I_{CaL} gating in the pathological conditions of OZR? Answers to these questions will provide us with mechanistic insights into cardiac arrhythmias associated with diabetes patients that are obese, which should have a significant impact in the prevention of sudden cardiac arrest in the increasing diabetes population.

ACKNOWLEDGMENTS

We thank Dr. Martin Myers (University of Michigan) for providing insulin receptor antibody as a generous gift. We are grateful for information of Cav1.2 antibody from Dr. Philip Palade (University of Arkansas for Medical Sciences).

GRANTS

Part of the work was supported by National Heart, Lung, and Blood Institute Grant HL-075023 and by the Office of Research and Graduate Programs/Health Sciences Center at West Virginia University (H.-G. Yu). J. Huang is the recipient of American Heart Association Fellowship Award.

DISCLOSURES

The authors declare that they have no conflict of interest. The findings and conclusions in this report are those of the authors and do not necessarily represent the views of the National Institute for Occupational Safety and Health.

REFERENCES

1. **Arikkath J, Campbell KP.** Auxiliary subunits: essential components of the voltage-gated calcium channel complex. *Curr Opin Neurobiol* 13: 298–307, 2003.
2. **Bevan P.** Insulin signalling. *J Cell Sci* 114: 1429–1430, 2001.
3. **Black DJ, Halling DB, Mandich DV, Pedersen SE, Altschuld RA, Hamilton SL.** Calmodulin interactions with IQ peptides from voltage-dependent calcium channels. *Am J Physiol Cell Physiol* 288: C669–C676, 2005.
4. **Catalucci D, Zhang DH, DeSantiago J, Aimond F, Barbara G, Chemin J, Bonci D, Picht E, Rusconi F, Dalton ND, Peterson KL, Richard S, Bers DM, Brown JH, Condorelli G.** Akt regulates L-type Ca^{2+} channel activity by modulating Cavalpha1 protein stability. *J Cell Biol* 184: 923–933, 2009.
5. **Catterall WA, Perez-Reyes E, Snutch TP, Striessnig J.** International Union of Pharmacology. XLVIII Nomenclature and structure-function relationships of voltage-gated calcium channels. *Pharmacol Rev* 57: 411–425, 2005.
6. **Cens T, Rousset M, Leyris JP, Fesquet P, Charnet P.** Voltage- and calcium-dependent inactivation in high voltage-gated Ca(2+) channels. *Prog Biophys Mol Biol* 90: 104–117, 2006.
7. **Colecraft HM, Alseikhan B, Takahashi SX, Chaudhuri D, Mittman S, Yegnasubramanian V, Alvania RS, Johns DC, Marban E, Yue DT.** Novel functional properties of Ca(2+) channel beta subunits revealed by their expression in adult rat heart cells. *J Physiol* 541: 435–452, 2002.
8. **Davies A, Hendrich J, Van Minh AT, Wratten J, Douglas L, Dolphin AC.** Functional biology of the alpha(2)delta subunits of voltage-gated calcium channels. *Trends Pharmacol Sci* 28: 220–228, 2007.
9. **Di Nardo F, Burattini R, Cogo CE, Faelli E, Ruggeri P.** Age-related analysis of insulin resistance, body weight and arterial pressure in the Zucker fatty rat. *Exp Physiol* 94: 162–168, 2009.
10. **Dolphin AC.** Beta subunits of voltage-gated calcium channels. *J Bioenerg Biomembr* 35: 599–620, 2003.
11. **Findlay I.** Physiological modulation of inactivation in L-type Ca^{2+} channels: one switch. *J Physiol* 554: 275–283, 2004.
12. **Foell JD, Balijepalli RC, Delisle BP, Yunker AM, Robia SL, Walker JW, McEnery MW, January CT, Kamp TJ.** Molecular heterogeneity of calcium channel beta-subunits in canine and human heart: evidence for differential subcellular localization. *Physiol Genomics* 17: 183–200, 2004.
13. **Ganesan AN, Maack C, Johns DC, Sidor A, O'Rourke B.** Beta-adrenergic stimulation of L-type Ca^{2+} channels in cardiac myocytes requires the distal carboxyl terminus of alpha1C but not serine 1928. *Circ Res* 98: e11–e18, 2006.
14. **Gill G, Woodward A, Casson I, Weston P.** Cardiac arrhythmia and nocturnal hypoglycaemia in type 1 diabetes-the 'dead in bed' syndrome revisited. *Diabetologia* 52: 42–45, 2009.
15. **Goldenberg I, Moss AJ.** Long QT syndrome. *J Am Coll Cardiol* 51: 2291–2300, 2008.
16. **Goldenberg I, Moss AJ, Zareba W.** QT interval: how to measure it and what is "normal." *J Cardiovasc Electrophysiol* 17: 333–336, 2006.
17. **Goodwill AG, Frisbee SJ, Stapleton PA, James ME, Frisbee JC.** Impact of chronic anticholesterol therapy on development of microvascular rarefaction in the metabolic syndrome. *Microcirculation* 200: 1–18, 2009.
18. **Grandi E, Pasqualini FS, Bers DM.** A novel computational model of the human ventricular action potential and Ca transient. *J Mol Cell Cardiol* 48: 112–121, 2010.
19. **Huang J, Huang A, Zhang Q, Lin YC, Yu HG.** Novel mechanism for suppression of hyperpolarization-activated cyclic nucleotide-gated pacemaker channels by receptor-like tyrosine phosphatase-α. *J Biol Chem* 283: 29912–29919, 2008.
20. **Jesmin S, Sakuma I, Hattori Y, Fujii S, Kitabatake A.** Long-acting calcium channel blocker benidipine suppresses expression of angiogenic growth factors and prevents cardiac remodelling in a Type II diabetic rat model. *Diabetologia* 45: 402–415, 2002.
21. **Junttila MJ, Barthel P, Myerburg RJ, Makikallio TH, Bauer A, Ulm K, Kiviniemi A, Tulppo M, Perkiomaki JS, Schmidt G, Huikuri HV.** Sudden cardiac death after myocardial infarction in patients with type 2 diabetes. *Heart Rhythm* 7: 1396–1403, 2010.
22. **Kereiakes DJ, Naughton JL, Brundage B, Schiller NB.** The heart in diabetes. *West J Med* 140: 583–593, 1984.

23. **Lebeche D, Davidoff AJ, Hajjar RJ.** Interplay between impaired calcium regulation and insulin signaling abnormalities in diabetic cardiomyopathy. *Nat Clin Pract Cardiovasc Med* 5: 715–724, 2008.
24. **Lin YC, Huang J, Zhang Q, Hollander JM, Frisbee JC, Martin KH, Nestor C, Goodman R, Yu HG.** Inactivation of L-type calcium channel modulated by HCN2 channel. *Am J Physiol Cell Physiol* 298: C1029–C1037, 2010.
25. **Lu Z, Jiang YP, Xu XH, Ballou LM, Cohen IS, Lin RZ.** Decreased L-type Ca^{2+} current in cardiac myocytes of type 1 diabetic Akita mice due to reduced phosphatidylinositol 3-kinase signaling. *Diabetes* 56: 2780–2789, 2007.
26. **Movahed MR, Hashemzadeh M, Jamal M.** Increased prevalence of ventricular fibrillation in patients with type 2 diabetes mellitus. *Heart Vessels* 22: 251–253, 2007.
27. **Pitt GS, Zuhlke RD, Hudmon A, Schulman H, Reuter H, Tsien RW.** Molecular basis of calmodulin tethering and Ca^{2+}-dependent inactivation of L-type Ca^{2+} channels. *J Biol Chem* 276: 30794–30802, 2001.
28. **Ren J, Sowers JR, Walsh MF, Brown RA.** Reduced contractile response to insulin and IGF-I in ventricular myocytes from genetically obese Zucker rats. *Am J Physiol Heart Circ Physiol* 279: H1708–H1714, 2000.
29. **Ren J, Walsh MF, Jefferson L, Natavio M, Ilg KJ, Sowers JR, Brown RA.** Basal and ethanol-induced cardiac contractile response in lean and obese Zucker rat hearts. *J Biomed Sci* 7: 390–400, 2000.
30. **Roden DM, Balser JR, George AL Jr, Anderson ME.** Cardiac ion channels. *Annu Rev Physiol* 64: 431–475, 2002.
31. **Sawicki PT, Dahne R, Bender R, Berger M.** Prolonged QT interval as a predictor of mortality in diabetic nephropathy. *Diabetologia* 39: 77–81, 1996.
32. **Shi W, Wymore R, Yu H, Wu J, Wymore RT, Pan Z, Robinson RB, Dixon JE, McKinnon D, Cohen IS.** Distribution and prevalence of hyperpolarization-activated cation channel (HCN) mRNA expression in cardiac tissues. *Circ Res* 85: e1–e6, 1999.
33. **Splawski I, Timothy KW, Sharpe LM, Decher N, Kumar P, Bloise R, Napolitano C, Schwartz PJ, Joseph RM, Condouris K, Tager-Flusberg H, Priori SG, Sanguinetti MC, Keating MT.** Ca(V)1.2 calcium channel dysfunction causes a multisystem disorder including arrhythmia and autism. *Cell* 119: 19–31, 2004.
34. **Stettler C, Bearth A, Allemann S, Zwahlen M, Zanchin L, Deplazes M, Christ ER, Teuscher A, Diem P.** QTc interval and resting heart rate as long-term predictors of mortality in type 1 and type 2 diabetes mellitus: a 23-year follow-up. *Diabetologia* 50: 186–194, 2007.
35. **Taggart P, Sutton PM, Boyett MR, Lab M, Swanton H.** Human ventricular action potential duration during short and long cycles. Rapid modulation by ischemia. *Circulation* 94: 2526–2534, 1996.
36. **Ter Keurs HE, Boyden PA.** Calcium and arrhythmogenesis. *Physiol Rev* 87: 457–506, 2007.
37. **Veglio M, Bruno G, Borra M, Macchia G, Bargero G, D'Errico N, Pagano GF, Cavallo-Perin P.** Prevalence of increased QT interval duration and dispersion in type 2 diabetic patients and its relationship with coronary heart disease: a population-based cohort. *J Intern Med* 251: 317–324, 2002.
38. **Veglio M, Giunti S, Stevens LK, Fuller JH, Perin PC.** Prevalence of Q-T interval dispersion in type 1 diabetes and its relation with cardiac ischemia: the EURODIAB IDDM Complications Study Group. *Diabetes Care* 25: 702–707, 2002.
39. **Witteles RM, Fowler MB.** Insulin-resistant cardiomyopathy clinical evidence, mechanisms, and treatment options. *J Am Coll Cardiol* 51: 93–102, 2008.
40. **Yarotskyy V, Elmslie KS.** Roscovitine, a cyclin-dependent kinase inhibitor, affects several gating mechanisms to inhibit cardiac L-type (Ca(V)1.2) calcium channels. *Br J Pharmacol* 152: 386–395, 2007.
41. **Yokoshiki H, Sumii K, Sperelakis N.** Inhibition of L-type calcium current in rat ventricular cells by the tyrosine kinase inhibitor, genistein and its inactive analog, daidzein. *J Mol Cell Cardiol* 28: 807–814, 1996.
42. **Yu H, Gao J, Wang H, Wymore R, Steinberg S, McKinnon D, Rosen MR, Cohen IS.** Effects of the renin-angiotensin system on the current I(to) in epicardial and endocardial ventricular myocytes from the canine heart. *Circ Res* 86: 1062–1068, 2000.
43. **Yu X, Chen XW, Zhou P, Yao L, Liu T, Zhang B, Li Y, Zheng H, Zheng LH, Zhang CX, Bruce I, Ge JB, Wang SQ, Hu ZA, Yu HGc-CA, Zhou Z.** Calcium influx through If channels in rat ventricular myocytes. *Am J Physiol Cell Physiol* 292: C1147–C1155, 2007.
44. **Zecchin HG, Bezerra RM, Carvalheira JB, Carvalho-Filho MA, Metze K, Franchini KG, Saad MJ.** Insulin signalling pathways in aorta and muscle from two animal models of insulin resistance–the obese middle-aged and the spontaneously hypertensive rats. *Diabetologia* 46: 479–491, 2003.